PUBLICATIONS OF THE ASTRONOMICAL SOCIETY OF THE PACIFIC, **117**:1236–1249, 2005 November

Identification of X-Ray Point Sources and a Study of the Nature of 62 X-Ray Globular Cluster Candidates in M31

ZHOU FAN, JUN MA, XU ZHOU, JIANSHENG CHEN, ZHAOJI JIANG, AND ZHENYU WU

National Astronomical Observatories, Chinese Academy of Sciences, Beijing 100012, China; majun@bac.pku.edu.cn

Received 2005 February 3; accepted 2005 July 12; published 2005 October 12

ABSTRACT. This paper includes two parts. The first presents the spectral energy distributions (SEDs) of 49 globular cluster (GC) X-ray sources in 13 BATC (Beijing-Arizona-Taiwan-Connecticut) intermediate-band filters from 3800 to 10000 Å, and identifies 8 previously unidentified X-ray sources in M31. Using X-ray data from *Einstein* observations from 1979 to 1980, *ROSAT* High Resolution Imager observations in 1990, *Chandra* High Resolution Channel and ACIS-I observations from 1999 to 2001, and the BATC optical survey from 1995 to 1999, we find 49 GC X-ray sources and 8 new X-ray sources in the BATC M31 field. By analyzing SEDs and FWHMs, we determine that 4 of the 8 X-ray sources may be GC candidates. The second part presents some statistical relationships between 62 GC X-ray sources, of which 58 are already known and 4 are identified in this paper. The distribution of M31's GC X-ray sources' V magnitudes is bimodal, with peaks at $m_v = 15.65$ and 17.89, which is different from the distribution of GC candidates. The distribution of $B - V$ color shows that the GC X-ray sources seem to be associated preferentially with the redder GCs, in agreement with previous results. Kolmogorov-Smirnov test shows that the maximum value of the absolute difference of $B - V$ distributions of GC X-ray sources and GCs is $D_{\max} = 0.181$, and the probability $P = 0.068$, which means we can reject the hypothesis that the two distributions are the same at the 90.0% confidence level. Finally, we study the correlation between X-ray luminosity (0.3–10 keV) and optical luminosity (in the V band) of the GC X-ray sources in M31, and find that there exits a weak relationship with the linear correlation coefficient $r = 0.36$ at a confidence level of 98.0%.

1. INTRODUCTION

In our Local Group, M31 is the nearest (780 kpc; Stanek & Garnavich 1998; Macri 2001) and largest spiral galaxy, containing hundreds of X-ray point sources (Supper et al. 1997, 2001). At the same time, M31 possesses many more globular clusters (GCs) than the Milky Way, with 435 GCs and GC candidates (Barmby et al. 2000). As we know, GC systems can provide important clues to our understanding of the evolution and history of galaxies. It is also clear that GCs are ideal laboratories for studying the populations and evolution of dense stellar systems (Trudolyubov & Priedhorsky 2004). X-ray surveys reveal that a number of bright X-ray sources associated with Milky Way GCs are identified as low-mass X-ray binaries (LMXBs; Hertz & Grindlay 1983). The ratio of LMXBs to stellar-mass objects is 2 orders of magnitude higher for GCs than for the rest of our Galaxy (Trudolyubov & Priedhorsky 2004; Liu et al. 2001). These LMXBs can be formed by capture from the remnants of massive single stars that exploded with sufficient isotropy to remain bound in GCs (Clark 1975), or via tidally dissipative two-body encounters in the dense cores of GCs (Fabian et al. 1975). However, the number of known Galactic GCs hosting bright X-ray sources is quite small; for example, there are only 14 X-ray GCs with luminosities above 10^{36} ergs s^{-1} identified in Liu et al. (2001). X-ray observations of M31 have been carried out many times, and hundreds of X-ray point sources have been discovered (van Speybroeck et al. 1979; Collura et al. 1990; Trinchieri & Fabbiano 1991; Primini et al. 1993; Trinchieri et al. 1999; Supper et al. 1997, 2001; Osborne et al. 2001; Kaaret 2002; Kong et al. 2002; Williams et al. 2004). With these observations, many optical counterparts of X-ray point sources in M31 have been detected; in a proportion greater than for GCs in the Milky Way. For example, in M31 about $\frac{1}{3}$ of the GC X-ray sources have luminosity $L_X \geq 10^{37}$ ergs s^{-1} (0.5–7.0 keV), compared to about $\frac{1}{12}$ within our Galaxy (Di Stefano et al. 2002a), and more than 30% of the GC X-ray sources in M31 have luminosity $L_X \geq 5 \times 10^{37}$ ergs s^{-1}, compared to only one in our Galaxy (Liu et al. 2001; Sidoli et al. 2001). Di Stefano et al. (2003) found that the optically bright X-ray GCs house only the brightest X-ray sources, and that X-ray sources are most likely to be found in red GCs.

Studying the correlation between optical and X-ray properties for GC X-ray sources is also important. At visual wavelengths, giants dominate the flux of GCs, low-mass main-sequence stars show up with deeper exposures, and X-ray observations detect compact objects (Verbunt et al. 1995). Bel-

lazzini et al. (1995) found that both Galactic and M31 GCs housing bright LMXBs are both denser and more metal rich. Trudolyubov & Priedhorsky (2004) later confirmed the conclusions of Bellazzini et al. (1995).

M31 was optically observed as part of a galaxy calibration program of the Beijing-Arizona-Taiwan-Connecticut (BATC) Multicolor Sky Survey (e.g., Fan et al. 1996; Zheng et al. 1999), which has a custom-designed set of 15 intermediate-band filters that perform spectrophotometry for preselected 1 deg^2 regions of the northern sky.

The outline of this paper is as follows. The X-ray data used are introduced in § 2. Details of optical observations and data reduction are given in § 3. Optical counterparts of X-ray point sources are identified in § 4. The nature of 62 GC X-ray sources is given in § 5. Finally, a summary is presented in § 6.

2. THE DATA OF X-RAY POINT SOURCES IN M31

Globular clusters of X-ray point sources used in this paper are mainly taken from Trudolyubov & Priedhorsky (2004), who presented the results of an M31 GC X-ray point-sources survey based on data from *XMM-Newton* and *Chandra* observations covering ~6100 arcmin^2 of M31, and detected 43 GC X-ray point sources. At the same time, in order to enlarge the number of GC X-ray point sources, we also refer to Trinchieri & Fabbiano (1991), Primini et al. (1993), Trinchieri et al. (1999), Supper et al. (2001), Kaaret (2002), Kong et al. (2002), and Williams et al. (2004). Trinchieri & Fabbiano (1991) reported the results of an entire set of *Einstein* imaging observations of M31 and detected 108 individual X-ray sources (0.2–4.0 keV). Primini et al. (1993) provided a report of a 48,000 s observation of the central ~34′ of M31 with the *ROSAT* High Resolution Imager (HRI) in 1990, in which they detected 86 X-ray sources with luminosities above $\sim 1.4 \times 10^{36}$ ergs s^{-1}, of which 18 were identified as GCs. Trinchieri et al. (1999) presented a spectral study of X-ray–emitting stellar sources in M31 and found that GC sources have spectral characteristics that are consistent with those of Milky Way objects. Supper et al. (2001) analyzed the second *ROSAT* survey of M31 within the ~10.7 deg^2 field of view and detected 396 individual X-ray point sources. Combined with the first survey, they presented 560 X-ray point sources, identifying 55 as foreground stars, 33 as GCs, 16 as supernova remnants (SNRs), and 10 as radio sources and galaxies. Using data from a deep observation of the core of M31, made with the *Chandra* High Resolution Channel (HRC; Murray et al. 1997), Kaaret (2002) detected 143 X-ray point sources, 20 of which were identified as GC candidates. By combining eight *Chandra* ACIS-I observations taken between 1999 and 2001, Kong et al. (2002) detected 204 X-ray sources within the central ~17′ × 17′ region, with a detection limit of $\sim 2.0 \times 10^{35}$ ergs s^{-1}. Of these X-ray sources, Kong et al. (2002) identified 45 counterparts: 22 GCs, 9 planetary nebulae (PNe), 2 SNRs, 9 supersoft sources (SSSs), and 3 stars. Williams et al. (2004) discovered 166 X-ray point sources, including 28 GCs, 17 stars, 1 BL Lacertae (BL), 6 PNe, and 3 SNRs, from the 17 epochs of *Chandra* HRC snapshot images, each covering most of the M31 disk. By comparing these papers, we find that there are 54 different GC X-ray point sources. In addition, we identify the optical counterparts of X-ray point sources using X-ray data on M31 from Trinchieri & Fabbiano (1991), Primini et al. (1993), Trinchieri et al. (1999), Kaaret (2002), Kong et al. (2002), and Williams et al. (2004), which present the positions of X-ray point sources, and also using optical BATC observations of M31.

3. THE BATC OPTICAL OBSERVATION OF M31

Optical observations of M31 were carried out by the BATC Multicolor Sky Survey system, which uses a 60/90 cm f/3 Schmidt telescope at the NAOC (National Astronomical Observatories of the Chinese Academy Sciences) Xinglong Station, where the seeing is ~2″. A Ford Aerospace 2k × 2k large-area CCD camera is mounted at the Schmidt telescope focus, giving a field of view of 58′ × 58′, with a pixel size of ~1.″67. This system includes 15 intermediate-band filters covering a wavelength range from 3000 to 10000 Å. In this work, only 13 intermediate-band filters (BATC03–BATC15, ~4000–10000 Å) are used. The optical observations of M31 were carried out from 1995 November 15 to 1999 December 16, and the total exposure lasted about 37 hr.

The calibrations of the images are made using observations of four *F* subdwarfs: HD 19445, HD 84937, BD +26 2606, and BD +17 4708, all taken from Oke & Gunn (1983). Hence, our magnitudes are defined in a way that is similar to the spectrophotometric AB magnitude system that is used for the Oke & Gunn $\tilde{f}_\nu$ monochromatic system. BATC magnitudes are defined on the AB magnitude system as

$$m_{\rm BATC} = -2.5 \log \tilde{F}_\nu - 48.60, \quad (1)$$

where $\tilde{F}_\nu$ is the appropriately averaged monochromatic flux in units of ergs s^{-1} cm^{-2} Hz^{-1} at the effective wavelength of the specific passband. In the BATC system (Yan et al. 2000), $\tilde{F}_\nu$ is defined as

$$\tilde{F}_\nu = \frac{\int d(\log \nu) f_\nu r_\nu}{\int d(\log \nu) r_\nu}, \quad (2)$$

which links the magnitude to the number of photons detected by the CCD, rather than to the input flux of Vega (Fukugita et al. 1996). In equation (2), r_ν is the system's response, and f_ν is the spectral energy distribution (SED) of the source.

Data reduction, beginning with the usual CCD processing steps of bias subtraction and flat-fielding with dome flats, was performed with the automatic data-reduction software PIPELINE I, which was developed for the BATC Multicolor Sky Survey (Fan et al. 1996; Zheng et al. 1999). The dome flat-field images were taken by using a diffuser plate in front of

the correcting plate of the Schmidt telescope, a flat-fielding technique that has been verified with photometry we have done on other galaxies and fields of view (e.g., Fan et al. 1996; Zheng et al. 1999; Wu et al. 2002; Yan et al. 2000; Zhou et al. 2001, 2004). Spectrophotometric calibration of the M31 images using the Oke-Gunn standard stars is done during photometric nights (see details from Yan et al. 2000; Zhou et al. 2001).

Using the images of standard stars observed on photometric nights, we iteratively derived the atmospheric extinction curves and the variations of these extinction coefficients with time (e.g., Zhou et al. 2001). The extinction coefficients at any given time of a night $[K + \Delta K(\mathrm{UT})]$, and the zero points of the instrumental magnitudes (C), are obtained by

$$m_{\mathrm{BATC}} = m_{\mathrm{inst}} + [K + \Delta K(\mathrm{UT})]X + C, \quad (3)$$

where X is the air mass. The instrumental magnitudes (m_{inst}) of the selected bright, isolated, and unsaturated stars on the M31 field images of the same photometric nights can be readily transformed to the BATC AB magnitude system (m_{BATC}). The calibrated magnitudes of these stars are obtained on the photometric nights, which are then used as secondary standards to uniformly combined images from calibrated nights to those taken during nonphotometric weather. Table 1 lists the parameters of the BATC filters and the statistics of the observations. Column (6) of Table 1 gives the scatter, in magnitudes, for the photometric observations of the four primary standard stars in each filter.

TABLE 1
PARAMETERS OF THE BATC FILTERS AND STATISTICS OF OBSERVATIONS FOR M31

Number (1)	Name (2)	CW (Å)[a] (3)	Exposure (hr) (4)	N[b] (5)	rms[c] (6)
1	BATC03	4210	01:00	3	0.015
2	BATC04	4546	05:30	17	0.009
3	BATC05	4872	03:30	11	0.015
4	BATC06	5250	02:20	12	0.006
5	BATC07	5785	02:15	7	0.003
6	BATC08	6075	01:40	5	0.003
7	BATC09	6710	00:45	3	0.003
8	BATC10	7010	03:00	12	0.008
9	BATC11	7530	02:00	6	0.004
10	BATC12	8000	04:00	12	0.003
11	BATC13	8510	01:30	5	0.004
12	BATC14	9170	05:50	18	0.003
13	BATC15	9720	04:00	12	0.009

[a] Central wavelength for each BATC filter.
[b] Image numbers for each BATC filter.
[c] Calibration error, in magnitude, for each filter as obtained from the standard stars.

4. IDENTIFICATION OF FOUR NEW GC X-RAY SOURCES

4.1. Finding Optical Counterparts of the GC X-Ray Sources

Trinchieri & Fabbiano (1991) presented the positions of 108 *Einstein* X-ray sources; Primini et al. (1993) listed the positions of 86 *ROSAT* HRI X-ray sources; and Kong et al. (2002), Kaaret (2002), and Williams et al. (2004) presented the positions of 204, 143, and 166 X-ray point sources using *Chandra*, ACIS-I, and HRC X-ray data, respectively. By comparing the positions of these X-ray point sources with the positions of objects in the BATC M31 field within a radius of $(2^2 + 2^2)^{1/2}$ pixels, we find that 17 X-ray point sources have optical counterparts in the BATC CCD images, in addition to the known optical counterparts in these papers. A search of the SIMBAD database reveals that nine X-ray sources have optical counterparts within a radius of 5″: CXOM31 J004216.0+411552, CXOM31 J004247.8+411052, CXOM31 J004301.7+411052, and RX J004138.3+410106 are identified as stars by Berkhuijsen et al. (1988); CXOM31 J004231.2+412008 is a GC candidate from Galleti et al. (2004); CXOM31 J004309.7+411901 and CXOM31 J004304.2+411601 are also GC candidates from Wirth et al. (1985); [GMP2000b] J004240.7+405117.7 is a planetary nebula from Ford & Jacoby (1978); and 2E 0041.3+4114 is a GC from Barmby et al. (2000). So only eight X-ray sources need to be identified, and every X-ray source has only one optical counterpart. Figure 1 shows the eight optical counterparts. The centers of the circles, each with a radius of $(2^2 + 2^2)^{1/2}$ pixels, are the position of the X-ray sources.

4.2. SEDs and FWHMs of GC X-Ray Sources

BATC multicolor photometry can provide the SED of an object. By analyzing the SED and FWHM of an object in the M31 field, we can determine whether or not it is a GC candidate. In general, we find that the mean FWHM value of an M31 GC is wider than that of a star in the Milky Way, the SEDs of GCs do not vary steeply from one BATC filter band to another, and the fluxes are greater in longer wavelengths. We first present the SEDs and mean FWHMs of the known GC X-ray point sources. Then, by comparing the SEDs and mean FWHMs to the known GC X-ray point sources and the optical counterparts of X-ray sources in the image of a BATC filter band, we can identify whether an optical counterpart of X-ray sources is a GC candidate or not.

Using the positions of the GC X-ray sources from Trinchieri & Fabbiano (1991), Primini et al. (1993), Trinchieri et al. (1999), Trudolyubov & Priedhorsky (2004), Kong et al. (2002), Williams et al. (2004), and Supper et al. (2001), and referring to the SIMBAD database, we found 49 individual GC X-ray sources in the BATC M31 field. For each GC X-ray point source, the PHOT routine in DAOPHOT (Stetson 1987) is used to obtain magnitudes. To avoid contamination from nearby objects, we adopt a small aperture of 10.″2, corresponding to a

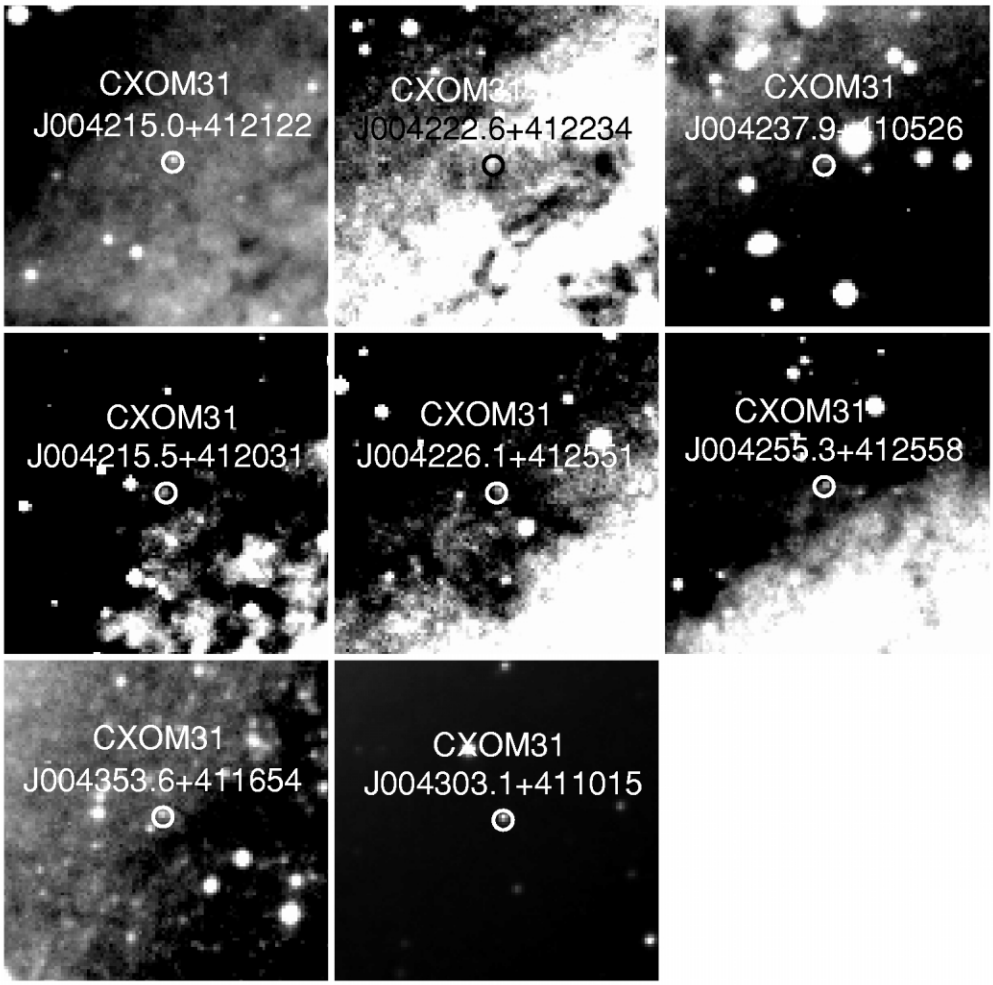

FIG. 1.—Finding charts for eight X-ray sources in M31. The centers of circles show the positions of X-ray sources.

diameter of 6 pixels in the Ford CCD. Large-aperture measurements of uncrowded bright stars were used to determine the aperture corrections; i.e., the magnitude difference between the small-aperture magnitude and the "total," or seeing-independent, magnitude for the stars on each frame. SEDs for 49 GC X-ray point sources in 13 BATC filters are obtained from these measurements. These data are given in Table 2. Columns (2)–(14) give the magnitudes of the 13 BATC passbands observed. The second line for each GC gives the 1 σ errors in magnitudes for the corresponding passband. The errors for each filter are given by DAOPHOT. Figure 2 plots the SEDs for these 49 GC X-ray sources. For convenience, in Figure 2 the flux ratios relative to filter BATC08 ($\lambda = 6075$ Å) are used, except for sources Bo D91/MIT236 and MIT311. For these two GCs, the flux ratios relative to BATC10 ($\lambda = 7010$ Å) are used, since they are very red.

In Table 3, we list the mean FWHM values of column and line direction for the 49 GC X-ray point sources in the BATC08 filter band. The mean FWHM values for MIT213 and PB-in7 cannot be fitted, because of low signal-to-noise ratio (S/N) or strong nearby background. We also list the mean FWHM values of column and line direction for eight Milky Way foreground stars around the GC X-ray point sources. The errors of FWHMs are the rms of FWHMs from eight Milky Way foreground stars. From Table 3, we can see that most of the GCs have larger FWHM values than those of nearby foreground stars.

4.3. SEDs and FWHMs of Eight New Optical Counterparts of X-Ray Point Sources

The PHOT routine in DAOPHOT (Stetson 1987) is used to obtain the magnitudes for each optical counterpart of an X-ray point source (see details from § 4.2). SEDs for optical counterparts in 13 BATC filters are obtained from these measurements and are listed in Table 4. Columns (2) to (14) list the

TABLE 2
THE SEDs OF 49 X-RAY GC CANDIDATES IN 13 BATC FILTER BANDS

Name (1)	BATC03 (4210 Å) (2)	BATC04 (4546 Å) (3)	BATC05 (4872 Å) (4)	BATC06 (5250 Å) (5)	BATC07 (5785 Å) (6)	BATC08 (6075 Å) (7)	BATC09 (6710 Å) (8)	BATC10 (7010 Å) (9)	BATC11 (7530 Å) (10)	BATC12 (8000 Å) (11)	BATC13 (8510 Å) (12)	BATC14 (9170 Å) (13)	BATC15 (9720 Å) (14)
Bo7	14.78	14.55	14.42	14.33	14.14	14.13	14.12	14.04	14.06	14.01	13.98	13.97	14.02
	0.011	0.004	0.003	0.003	0.003	0.002	0.002	0.003	0.003	0.003	0.004	0.008	0.013
MIT87	19.85	19.77	19.33	19.18	18.85	18.90	18.80	18.81	18.80	18.62	19.12	18.45	18.70
	0.155	0.174	0.115	0.123	0.116	0.115	0.148	0.175	0.218	0.201	0.510	0.292	0.455
Bo45	16.75	16.37	16.11	15.91	15.55	15.49	15.29	15.18	15.09	14.96	14.90	14.83	14.73
	0.057	0.016	0.010	0.008	0.007	0.006	0.004	0.007	0.007	0.006	0.008	0.016	0.024
Bo55	18.99	17.70	17.19	16.85	16.42	16.22	15.94	15.77	15.59	15.42	15.27	15.05	14.99
	0.407	0.068	0.040	0.030	0.028	0.023	0.021	0.022	0.022	0.019	0.021	0.027	0.036
Bo D42/MIT130	19.70	19.24	18.81	18.77	18.43	18.34	18.22	18.02	17.89	17.51	18.03	17.48	17.66
	0.091	0.073	0.058	0.083	0.084	0.080	0.099	0.096	0.107	0.083	0.211	0.121	0.178
Bo D44	18.83	19.62	19.09	18.66	18.12	17.79	17.69	17.45	17.26	17.00	16.29	16.70	16.69
	0.068	0.190	0.138	0.097	0.077	0.051	0.060	0.054	0.054	0.045	0.034	0.048	0.063
MIT140	18.61	18.02	17.38	17.05	16.47	16.26	15.91	15.67	15.38	15.25	15.09	14.83	14.87
	0.316	0.125	0.081	0.069	0.057	0.050	0.044	0.044	0.041	0.038	0.037	0.044	0.046
Bo78/MIT153	20.01	18.88	18.39	17.99	17.37	17.28	16.86	16.69	16.46	16.28	16.09	15.91	15.86
	0.521	0.295	0.262	0.214	0.177	0.178	0.146	0.141	0.133	0.129	0.121	0.113	0.110
Bo82/MIT159	17.58	16.76	16.20	15.78	15.17	14.99	14.60	14.40	14.15	14.00	13.85	13.64	13.61
	0.119	0.028	0.015	0.012	0.008	0.007	0.004	0.006	0.005	0.004	0.005	0.007	0.011
Bo86/MIT164	15.72	15.46	15.22	15.09	14.82	14.77	14.65	14.57	14.49	14.45	14.37	14.32	14.34
	0.036	0.037	0.042	0.040	0.039	0.039	0.039	0.043	0.048	0.045	0.046	0.063	0.055
MIT165/MIT166	19.82	19.62	19.18	18.34	18.09	18.05	17.76	17.83	17.56	17.36	17.16	17.02	16.89
	0.897	0.367	0.212	0.106	0.123	0.109	0.103	0.142	0.141	0.117	0.127	0.182	0.214
Bo94/MIT173	16.42	16.09	15.84	15.67	15.33	15.25	15.05	14.93	14.79	14.72	14.63	14.50	14.49
	0.041	0.015	0.011	0.009	0.009	0.007	0.005	0.008	0.008	0.006	0.009	0.014	0.022
Bo98	17.17	16.76	16.49	16.32	16.03	15.97	15.76	15.68	15.61	15.56	15.48	15.35	15.39
	0.011	0.007	0.007	0.007	0.007	0.006	0.007	0.007	0.008	0.007	0.014	0.011	0.017
Bo96/MIT174	17.43	16.97	16.47	16.31	15.90	15.82	15.59	15.40	15.23	15.18	15.09	14.88	15.09
	0.148	0.118	0.113	0.111	0.098	0.095	0.094	0.093	0.096	0.087	0.089	0.102	0.104
Bo D63	19.45	18.75	18.62	18.80	18.37	18.48	18.66	18.96	18.76	18.86	18.29	…	18.67
	0.068	0.148	0.092	0.108	0.093	0.086	0.096	0.245	0.240	0.212	0.201	…	0.841
Bo110	16.03	15.68	15.41	15.25	14.96	14.88	14.69	14.59	14.48	14.40	14.31	14.20	14.20
	0.029	0.011	0.008	0.007	0.007	0.006	0.005	0.007	0.007	0.007	0.008	0.012	0.017
Bo117	16.96	16.67	16.39	16.30	16.07	15.99	15.82	15.77	15.68	15.67	15.60	15.45	15.58
	0.068	0.030	0.016	0.016	0.031	0.016	0.012	0.017	0.017	0.017	0.025	0.032	0.061
Bo107/MIT192	16.98	16.46	16.18	16.02	15.62	15.53	15.32	15.24	15.13	15.03	14.95	14.84	14.84
	0.097	0.075	0.082	0.081	0.073	0.069	0.072	0.079	0.086	0.076	0.079	0.104	0.090
NBol 63	17.53	17.19	16.81	16.77	16.63	16.60	16.52	16.46	16.40	16.48	16.54	16.39	16.64
	0.108	0.117	0.119	0.125	0.156	0.162	0.169	0.183	0.199	0.254	0.312	0.275	0.348
Bo116	18.56	17.76	17.32	17.05	16.50	16.31	15.96	15.80	15.55	15.38	15.21	14.99	14.93
	0.313	0.054	0.029	0.024	0.021	0.015	0.011	0.015	0.014	0.011	0.014	0.019	0.030
Bo123/MIT212	18.37	17.97	17.61	17.51	17.07	17.01	16.78	16.76	16.62	16.49	16.33	16.20	16.03
	0.278	0.180	0.191	0.200	0.179	0.174	0.178	0.208	0.230	0.203	0.198	0.259	0.198
MIT213	14.49	13.97	13.53	13.40	13.06	12.98	12.75	12.62	12.38	12.38	12.25	11.91	12.05
	0.141	0.147	0.151	0.151	0.149	0.147	0.147	0.152	0.155	0.153	0.152	0.162	0.155
PB-in7	15.95	15.31	14.92	14.80	14.51	14.48	14.28	14.10	13.89	13.91	13.79	13.39	13.63
	0.237	0.221	0.238	0.240	0.247	0.256	0.262	0.264	0.275	0.277	0.276	0.282	0.289
Bo128	17.85	17.38	17.03	16.91	16.68	16.57	16.45	16.26	16.12	16.01	15.83	15.73	15.77
	0.094	0.089	0.086	0.087	0.098	0.095	0.098	0.095	0.101	0.112	0.103	0.100	0.110
Bo135	16.83	16.56	16.28	16.06	15.70	15.64	15.45	15.34	15.25	15.14	15.06	14.93	14.90
	0.060	0.020	0.014	0.012	0.011	0.010	0.009	0.012	0.013	0.011	0.014	0.019	0.030
Bo138	17.20	16.46	16.20	15.99	15.64	15.53	15.42	15.26	15.00	14.98	14.99	14.60	14.86
	0.228	0.180	0.213	0.194	0.187	0.176	0.192	0.198	0.194	0.188	0.213	0.221	0.234
Bo144	17.44	16.60	16.32	16.21	15.79	15.78	15.56	15.42	15.25	15.22	15.14	14.80	14.89
	0.268	0.198	0.235	0.244	0.225	0.233	0.237	0.252	0.271	0.260	0.277	0.294	0.269
Bo143	16.91	16.46	16.23	16.06	15.69	15.60	15.36	15.25	15.06	14.97	14.83	14.69	14.71
	0.102	0.076	0.091	0.090	0.090	0.087	0.086	0.098	0.103	0.092	0.092	0.121	0.100
Bo146	17.77	17.38	17.29	16.93	16.66	16.63	16.31	16.14	15.95	15.92	15.83	15.70	15.67
	0.254	0.252	0.345	0.287	0.300	0.311	0.280	0.293	0.304	0.295	0.301	0.400	0.325

TABLE 2 (*Continued*)

Name (1)	BATC03 (4210 Å) (2)	BATC04 (4546 Å) (3)	BATC05 (4872 Å) (4)	BATC06 (5250 Å) (5)	BATC07 (5785 Å) (6)	BATC08 (6075 Å) (7)	BATC09 (6710 Å) (8)	BATC10 (7010 Å) (9)	BATC11 (7530 Å) (10)	BATC12 (8000 Å) (11)	BATC13 (8510 Å) (12)	BATC14 (9170 Å) (13)	BATC15 (9720 Å) (14)
Bo D91/MIT236	15.81	15.25	14.36	14.17	14.26	14.31	12.30	13.53	13.20	13.27	13.14	12.59	13.31
	0.024	0.009	0.004	0.004	0.005	0.005	0.001	0.004	0.004	0.004	0.004	0.005	0.009
Bo147/MIT240	16.64	16.11	15.82	15.68	15.33	15.24	15.06	14.92	14.73	14.68	14.57	14.43	14.43
	0.075	0.055	0.058	0.056	0.052	0.047	0.046	0.049	0.049	0.043	0.043	0.054	0.047
Bo148	16.62	16.31	16.13	15.90	15.60	15.53	15.32	15.24	15.07	14.99	14.89	14.77	14.84
	0.078	0.071	0.090	0.086	0.088	0.088	0.087	0.100	0.110	0.099	0.104	0.136	0.122
[WSB85] S3 14	17.48	17.21	16.86	16.91	16.36	16.29	16.34	16.03	15.79	15.51	15.36	15.35	15.36
	0.119	0.152	0.157	0.178	0.162	0.163	0.194	0.172	0.169	0.160	0.162	0.161	0.174
Bo150/MIT246	17.53	16.99	16.63	16.41	16.04	15.95	15.77	15.61	15.39	15.31	15.22	14.98	15.06
	0.161	0.117	0.113	0.097	0.087	0.082	0.078	0.081	0.079	0.071	0.071	0.085	0.082
[WSB85] S1 4	19.64	18.99	18.32	18.10	17.62	17.51	17.12	17.05	16.73	16.64	16.58	16.26	16.39
	0.523	0.427	0.323	0.279	0.256	0.243	0.193	0.209	0.189	0.205	0.220	0.173	0.202
Bo153/MIT251	17.55	16.74	16.44	16.25	15.91	15.84	15.65	15.58	15.32	15.28	15.17	15.02	15.05
	0.143	0.078	0.087	0.079	0.076	0.073	0.077	0.085	0.082	0.078	0.079	0.102	0.092
Bo158	15.61	15.20	14.91	14.75	14.42	14.35	14.16	14.09	13.96	13.89	13.81	13.71	13.67
	0.019	0.007	0.004	0.004	0.004	0.003	0.002	0.004	0.004	0.003	0.005	0.007	0.010
Bo161/MIT260	17.03	16.85	16.52	16.35	16.07	16.01	15.85	15.76	15.68	15.60	15.54	15.52	15.58
	0.078	0.039	0.035	0.032	0.032	0.030	0.030	0.034	0.038	0.034	0.039	0.056	0.069
Bo159	18.29	17.79	17.19	17.06	16.75	16.58	16.41	16.21	15.93	15.96	15.92	15.54	15.78
	0.241	0.097	0.067	0.064	0.058	0.045	0.043	0.045	0.043	0.042	0.048	0.057	0.086
Bo164	18.62	18.35	17.92	17.85	17.51	17.48	17.24	17.11	16.98	16.87	16.78	16.42	16.35
	0.288	0.130	0.100	0.104	0.105	0.098	0.094	0.108	0.119	0.106	0.123	0.133	0.145
Bo163	16.18	15.66	15.34	15.16	14.79	14.68	14.48	14.37	14.17	14.10	13.99	13.76	13.77
	0.033	0.012	0.009	0.007	0.007	0.006	0.005	0.007	0.007	0.006	0.007	0.008	0.013
Bo182	16.38	16.04	15.75	15.53	15.16	15.10	14.86	14.77	14.63	14.51	14.41	14.27	14.26
	0.038	0.013	0.008	0.007	0.006	0.006	0.004	0.007	0.007	0.005	0.007	0.012	0.017
Bo185/MIT299	16.53	16.11	15.81	15.66	15.30	15.24	15.05	14.97	14.81	14.73	14.68	14.56	14.52
	0.040	0.015	0.011	0.010	0.010	0.009	0.009	0.011	0.012	0.011	0.012	0.018	0.024
MIT311	19.13	19.37	19.23	18.68	18.01	17.82	17.52	17.26	17.05	16.95	16.65	16.68	16.22
	0.494	0.305	0.248	0.155	0.106	0.086	0.063	0.066	0.061	0.060	0.057	0.106	0.095
Bo193	16.47	15.98	15.70	15.53	15.12	15.03	14.85	14.73	14.53	14.47	14.39	14.19	14.16
	0.043	0.012	0.009	0.007	0.007	0.005	0.004	0.006	0.006	0.005	0.008	0.010	0.016
Bo204	16.63	16.24	15.97	15.82	15.46	15.37	15.20	15.10	14.98	14.88	14.85	14.70	14.65
	0.049	0.016	0.011	0.009	0.009	0.008	0.007	0.009	0.011	0.009	0.012	0.018	0.026
Bo213	17.92	17.42	17.13	16.94	16.79	16.51	16.40	16.31	16.08	15.93	15.99	15.84	15.77
	0.027	0.022	0.020	0.017	0.023	0.017	0.019	0.018	0.019	0.018	0.026	0.024	0.028
MA94a(380)	15.73	15.31	15.03	14.91	14.53	14.48	14.36	14.27	14.19	14.14	14.09	14.01	14.01
	0.021	0.008	0.005	0.005	0.005	0.004	0.003	0.005	0.005	0.004	0.006	0.009	0.015
Bo225	15.12	14.71	14.42	14.32	13.91	13.81	13.63	13.52	13.34	13.27	13.20	13.05	13.04
	0.014	0.005	0.004	0.003	0.003	0.002	0.002	0.003	0.003	0.002	0.003	0.005	0.007

NOTES.—Source identifications beginning with Bo refer to the GC candidates listed in Battistini et al. (1987); Bo D to Battistini et al. (1980); MIT to Magnier (1993); NBol to Battistini et al. (1993); and PB to Barmby (2001). Source identifications beginning with [WSB85] refers to the list of GC X-ray sources listed in Wirth et al. (1985). Errors are given below each value.

magnitudes in 13 BATC passbands. The second line lists the 1 σ errors of magnitude for the corresponding passband, which are obtained from DAOPHOT. Figure 3 plots the SEDs for eight optical counterparts in 13 BATC filters. For convenience, we also calculated the flux ratios relative to the BATC08 filter ($\lambda = 6075$ Å), as in Figure 2, except for CXOM31 J004237.9+410526. For this optical counterpart, the flux ratios relative to the BATC10 filter ($\lambda = 7010$ Å) are used, since the source is very red.

Table 5 lists the mean FWHM values of column and line direction for the optical counterparts in the BATC08 filter band. Column (1) lists the name of the X-ray sources. Columns (2) and (3) list the R.A. and decl. of the sources, respectively, and column (4) gives the mean FWHM values (for column and line direction) of the optical counterparts of the X-ray sources. Column (5) lists the mean FWHM values of column and line direction for eight Milky Way foreground stars around every X-ray point source. The errors of the FWHMs are the rms of FWHMs from eight Milky Way foreground stars. Column (10) lists the radial offsets between the X-ray sources and their optical counterparts. For CXOM31 J004222.6+412234 and CXOM31 J004255.3+412558, which are two very faint objects with strong

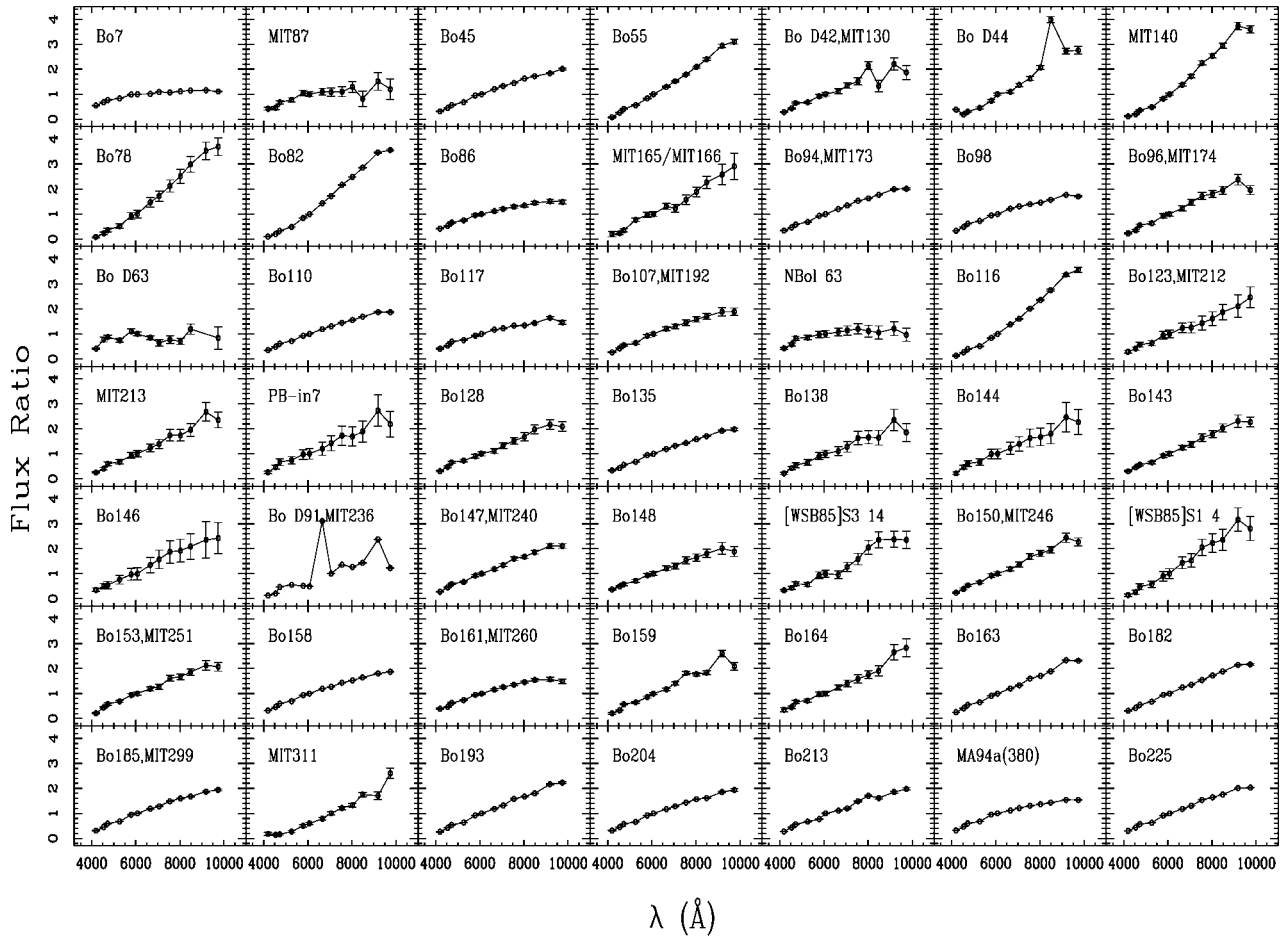

FIG. 2.—SEDs of 49 known GC X-ray point sources in M31.

backgrounds, estimates of their FWHMs are uncertain, so we did not give the them for these two objects, and did not identify them. So there are six X-ray sources left to be identified. We use the 49 known GC X-ray sources as template SEDs and compare the SED of each optical counterpart with the 49 template SEDs using the χ^2 method, and choose the one with the minimum value of χ^2:

$$\chi^2 = \sum_{i=3}^{15} \frac{[C_{\lambda_i}^{\rm new}(m) - C_{\lambda_i}^{\rm temp}(n)]^2}{\sigma_i^2(m) + \sigma_i^2(n)}, \qquad (4)$$

where $C_{\lambda_i}^{\rm temp}(n)$ represents the flux ratio in the ith filter (relative to filter BATC08; $\lambda = 6075$ Å) of the nth template GC X-ray source, and $\sigma_i^{\rm temp}(n)$ is the corresponding observational flux uncertainty in the ith filter of the nth template GC X-ray source obtained from the magnitude uncertainty. The expressions $C_{\lambda_i}^{\rm new}(m)$ and $\sigma_i^{\rm temp}(m)$ have similar meanings, but are for the mth new optical counterparts of the X-ray source that need to be identified. In addition, we have calculated the probability Q. The minimum values of χ^2 ($\chi^2_{\rm min}$) and the corresponding Q are listed in columns (7) and (8), respectively, of Table 5. We identify new optical counterparts of X-ray point sources as GC candidates, as explained below. First, when Q is smaller than 0.1, we reject the hypothesis that the candidate SED and the template are consistent, as Lampton et al. (1976) argued. Second, the mean FWHM value of a X-ray GC candidate should be no less than those of the nearby foreground stars. The optical counterparts identified as GC candidates are indicated in column (9), and the names of the template GC X-ray sources with the minimum values of χ^2 are listed in column (6).

5. THE PROPERTIES OF 62 GC CANDIDATES OF X-RAY SOURCES

In this section, we study the properties of 62 GC X-ray sources.

5.1. The Sample of 62 GC Candidates of X-Ray Sources

There are 58 known GC candidates of X-ray sources found in the literatures: 43 are from Trudolyubov & Priedhorsky

TABLE 3
THE FWHM OF 49 X-RAY GC CANDIDATES IN BATC08 FILTER BAND

Optical Name	FWHMs (GCs) (pixel)	FWHMs (stars) (pixel)
Bo7	2.5 ± 0.14	2.4 ± 0.14
MIT87	4.3 ± 0.45	2.7 ± 0.45
Bo45	2.7 ± 0.05	2.2 ± 0.05
Bo55	2.8 ± 0.23	2.1 ± 0.23
Bo D42/MIT130	3.5 ± 0.18	2.6 ± 0.18
Bo D44	3.8 ± 0.02	2.6 ± 0.02
MIT140	2.6 ± 0.21	2.4 ± 0.21
Bo78/MIT153	2.5 ± 0.21	2.4 ± 0.21
Bo82/MIT159	3.1 ± 0.13	2.6 ± 0.13
Bo86/MIT164	2.6 ± 0.24	2.3 ± 0.24
MIT165/MIT166	3.4 ± 0.12	2.0 ± 0.12
Bo94/MIT173	3.3 ± 0.09	2.5 ± 0.09
Bo98	3.0 ± 0.09	2.5 ± 0.09
Bo96/MIT174	3.4 ± 0.10	2.0 ± 0.10
Bo D63	3.1 ± 0.02	2.9 ± 0.02
Bo110	2.8 ± 0.06	2.5 ± 0.06
Bo117	3.3 ± 0.09	2.5 ± 0.09
Bo107/MIT192	2.3 ± 0.10	2.0 ± 0.10
NBol 63	2.8 ± 0.10	2.0 ± 0.10
Bo116	2.5 ± 0.02	2.1 ± 0.02
Bo123/MIT212	2.9 ± 0.04	2.4 ± 0.04
MIT213	…	…
PB-in7	…	…
Bo128	2.2 ± 0.04	2.4 ± 0.04
Bo135	2.4 ± 0.24	2.2 ± 0.24
Bo138	3.4 ± 0.12	2.3 ± 0.12
Bo144	2.7 ± 0.03	2.3 ± 0.03
Bo143	2.7 ± 0.12	2.3 ± 0.12
Bo146	3.5 ± 0.03	2.3 ± 0.03
Bo D91/MIT236	3.2 ± 0.24	2.1 ± 0.24
Bo147/MIT240	2.8 ± 0.06	2.1 ± 0.06
Bo148	2.7 ± 0.08	2.3 ± 0.08
[WSB85] S3 14	2.4 ± 0.03	2.3 ± 0.03
Bo150/MIT246	2.8 ± 0.06	2.1 ± 0.06
[WSB85] S1 4	2.7 ± 0.08	2.3 ± 0.08
Bo153/MIT251	2.4 ± 0.03	2.3 ± 0.03
Bo158	2.8 ± 0.02	2.3 ± 0.02
Bo161/MIT260	2.6 ± 0.02	2.3 ± 0.02
Bo159	3.0 ± 0.04	2.1 ± 0.04
Bo164	2.5 ± 0.03	2.3 ± 0.03
Bo163	2.6 ± 0.04	2.1 ± 0.04
Bo182	3.0 ± 0.02	2.3 ± 0.02
Bo185/MIT299	2.5 ± 0.03	2.3 ± 0.03
MIT311	2.8 ± 0.03	2.2 ± 0.03
Bo193	2.8 ± 0.34	1.9 ± 0.34
Bo204	2.5 ± 0.11	2.2 ± 0.11
Bo213	2.4 ± 0.05	2.4 ± 0.05
MA94a(380)	2.3 ± 0.20	2.2 ± 0.20
Bo225	2.7 ± 0.01	2.3 ± 0.01

(2004), 7 from Supper et al. (2001), 2 from Williams et al. (2004), 1 from Kong et al. (2002), 1 from Kong et al. (2002) and Galleti et al. (2004), 1 from Kaaret (2002) and Wirth et al. (1985), 1 from Williams et al. (2004) and Wirth et al. (1985), 1 from Primini et al. (1993), and 1 from Trinchieri & Fabbiano (1991) and Barmby et al. (2000). In order to enlarge the sample of GC candidates of X-ray sources, we also add four GC candidates identified from this paper. Therefore, there are 62 GC candidates of X-ray sources in all. Figure 4 shows the space distribution of the sources in the BATC M31 field (the circles represent the known GC X-ray sources, while the squares represent the newly identified GC X-ray candidates). There are 9 sources that are outside of the BATC M31 field or are too dim to be detected, so only 53 are shown in Figure 4.

In Table 6, we list some parameters of the 58 known GC candidates of X-ray sources from Trinchieri & Fabbiano (1991), Primini et al. (1993), Supper et al. (2001), Kaaret (2002), Kong et al. (2002), Williams et al. (2004), and Trudolyubov & Priedhorsky (2004), and the 4 new ones identified in this paper. Column (1) gives the number, column (2) lists the optical names, column (3) lists the names of X-ray sources, and column (4) lists the X-ray luminosities, given in units of 10^{35} ergs s^{-1}. The X-ray sources from Trudolyubov & Priedhorsky (2004) are observed in the 0.3–10 keV energy band, those of Supper et al. (2001) are 0.1–2 keV, those of Kong et al. (2002) and Williams et al. (2004) are 0.3–7 keV, those ofKaaret (2002) are 0.1–10 keV, and Trinchieri & Fabbiano (1991) and Primini et al. (1993) are 0.2–4.0 keV.

5.2. *B*, *V* Magnitude and $B - V$ Color of 58 GC Candidates of X-Ray Sources

Using the Landolt standards, Zhou et al. (2003) presented the relationships between the BATC intermediate-band system and the *UBVRI* broadband system from the catalogs of Landolt (1983, 1992) and Galadí-Enríquez et al. (2000). We show the coefficients of two relationships in equations (5) and (6):

$$m_B = m_{\rm BATC04} + 0.2201(m_{\rm BATC03} - m_{\rm BATC05}) + 0.1278 \pm 0.076, \quad (5)$$

$$m_V = m_{\rm BATC07} + 0.3292(m_{\rm BATC06} - m_{\rm BATC08}) + 0.0476 \pm 0.027. \quad (6)$$

The uncertainties in B (BATC) and V (BATC) are calculated as $\sigma_B = [\sigma^2_{\rm BATC04} + 0.2201^2(\sigma^2_{\rm BATC03} + \sigma^2_{\rm BATC05})]^{1/2}$ and $\sigma_V = [\sigma^2_{\rm BATC07} + 0.3292^2(\sigma^2_{\rm BATC06} + \sigma^2_{\rm BATC08})]^{1/2}$, to reflect the errors in the three filter measurements. For the colors, we add the errors in quadrature; i.e., $\sigma_{B-V} = (\sigma_B^2 + \sigma_V^2)^{1/2}$.

Using the equations above, we transformed the magnitudes of 53 GC candidates of X-ray sources in the BATC03, BATC04, and BATC05 bands to the B band, and the BATC06, BATC07, and BATC08 bands to the V band. For the other 9 sources that are outside of the BATC M31 field or cannot be detected in the BATC M31 field, we can find V magnitudes and $B - V$ colors of the 5 from Battistini et al. (1987). In all, there are 58 GC X-ray sources with V magnitudes and $B - V$ colors.

The fact that the GCs hosting X-ray sources tend to be op-

TABLE 4
THE SEDs OF EIGHT X-RAY OPTICAL COUNTERPARTS IN 13 BATC FILTER BANDS

Name (1)	BATC03 (4210 Å) (2)	BATC04 (4546 Å) (3)	BATC05 (4872 Å) (4)	BATC06 (5250 Å) (5)	BATC07 (5785 Å) (6)	BATC08 (6075 Å) (7)	BATC09 (6710 Å) (8)	BATC10 (7010 Å) (9)	BATC11 (7530 Å) (10)	BATC12 (8000 Å) (11)	BATC13 (8510 Å) (12)	BATC14 (9170 Å) (13)	BATC15 (9720 Å) (14)
CXOM31 J004215.0+412122	19.02	18.80	18.49	18.45	18.14	18.08	18.01	17.92	17.78	17.77	17.65	17.45	17.43
	0.066	0.060	0.056	0.068	0.078	0.072	0.099	0.105	0.115	0.137	0.155	0.147	0.178
CXOM31 J004222.6+412234	19.99	19.59	19.32	19.20	19.25	19.36	19.72	20.19	20.79	21.34	21.01	20.17	18.84
	0.256	0.197	0.206	0.187	0.250	0.258	0.433	0.724	1.455	2.639	2.292	1.480	0.515
CXOM31 J004237.9+410526	20.92	20.08	20.01	19.49	18.92	18.95	18.14	17.83	17.33	17.21	16.99	16.68	16.65
	0.436	0.287	0.385	0.260	0.206	0.208	0.127	0.107	0.083	0.081	0.101	0.069	0.080
CXOM31 J004215.5+412031	19.21	18.97	18.70	18.81	18.54	18.65	18.61	18.52	18.61	18.61	19.55	18.28	18.58
	0.138	0.147	0.148	0.183	0.197	0.228	0.253	0.265	0.359	0.422	1.277	0.413	0.626
CXOM31 J004226.1+412551	19.90	20.03	19.84	20.00	19.82	20.14	19.51	19.58	19.40	20.03	19.81	21.25	19.28
	0.151	0.199	0.211	0.277	0.354	0.476	0.326	0.408	0.475	0.899	1.003	4.407	0.847
CXOM31 J004255.3+412558	20.48	19.51	19.34	19.16	18.67	18.62	18.65	18.49	18.33	18.42	17.97	18.04	18.71
	0.485	0.280	0.335	0.306	0.284	0.281	0.336	0.322	0.313	0.386	0.305	0.340	0.646
CXOM31 J004353.6+411654	18.51	18.43	18.23	18.24	18.12	18.08	18.15	18.05	18.08	18.03	17.85	17.80	17.87
	0.088	0.088	0.078	0.086	0.104	0.094	0.116	0.122	0.154	0.156	0.162	0.163	0.213
CXOM31 J004303.1+411015	16.69	15.98	15.63	15.52	15.06	14.97	14.81	14.72	14.65	14.58	14.46	14.44	14.46
	0.010	0.007	0.007	0.007	0.007	0.007	0.007	0.008	0.009	0.010	0.012	0.011	0.014

tically brighter than the rest of the M31 GCs has been noted by Di Stefano et al. (2002b) and Trudolyubov & Priedhorsky (2004). Sarazin et al. (2003) also found a strong tendency for the X-ray sources to be associated with the optically more luminous GCs in four early-type galaxies. With the expanded sample of GC X-ray sources, Figure 5 plots the distribution of *V* magnitudes for the GC candidates of X-ray sources, along with the distribution for the whole sample of the class A and B GC candidates from Battistini et al. (1987). For clarity, we use the normalized number; i.e., in each bin the number of objects is divided by the number of all the objects. From this figure, we can see that these two distributions are not the same. The majority of GC X-ray sources are brighter than 17 mag, which is the peak of the distribution of the GC candidates. This conclusion is in agreement with that found by Di Stefano et al. (2002b) and Trudolyubov & Priedhorsky (2004). At the same time, the *V* magnitude distribution of the GC X-ray sources can be clearly seen to be bimodal; i.e., besides the major brighter GCs hosting X-ray sources that confirm the conclusions of Di Stefano et al. (2002b) and Trudolyubov & Priedhorsky (2004), there are also some GC X-ray sources that are less luminous. The fact that the GCs hosting X-ray sources tend to be optically brighter than the rest of the M31 GCs seems to be a result primarily of the larger number of stars in optically luminous GCs (Sarazin et al. 2003). As for the result that there are some less luminous GC X-ray sources, it is interesting but still needs to be confirmed with a larger sample.

To make quantitative statements about the bimodality of *V* magnitudes for GC X-ray sources, the KMM test (Ashman et al. 1994) is applied to the data. This test uses a maximum-likelihood method to estimate the probability that the data distribution is better modeled as a sum of two Gaussians rather than

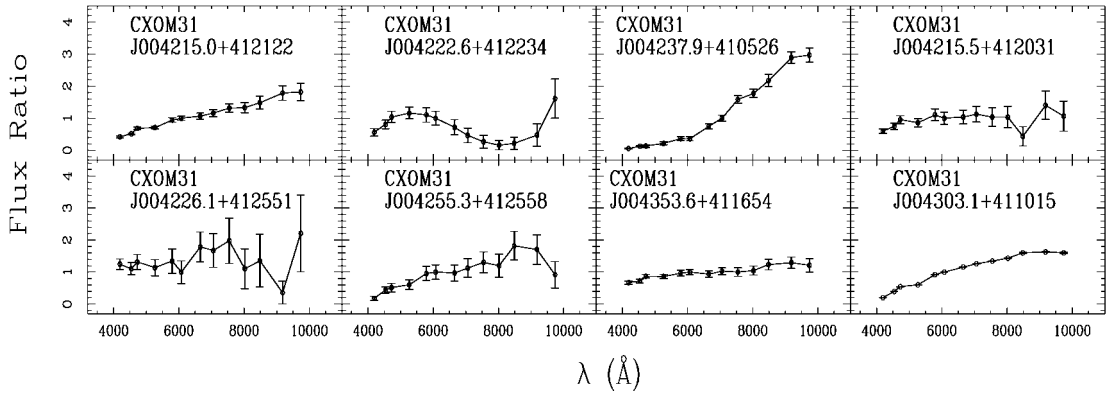

FIG. 3.—SEDs of the eight previously unidentified optical counterparts of X-ray point sources.

TABLE 5
THE IDENTIFICATION OF FOUR X-RAY GC CANDIDATES IN M31

Name (1)	R.A. (J2000.0) (2)	Decl. (J2000.0) (3)	FWHM of Sources (pixels) (4)	FWHM of Stars (pixels) (5)	Known X-ray GCs (6)	χ^2_{min} (7)	Q (8)	Type (9)	Radial Offset (arcsec) (10)
CXOM31 J004215.0+412122	00 42 15.03	+41 21 22.0	2.4 ± 0.04	2.1 ± 0.04	Bo86/MIT164	3.66	0.988	GC	4.15
CXOM31 J004222.6+412234	00 42 22.62	+41 22 34.9	…	…	…	…	…	…	3.60
CXOM31 J004237.9+410526	00 42 37.94	+41 05 26.1	2.6 ± 0.06	2.5 ± 0.06	Bo146	149.20	0.000	…	2.84
CXOM31 J004215.5+412031	00 42 15.53	+41 20 31.9	3.3 ± 0.11	2.1 ± 0.11	Bo7	5.51	0.938	GC	2.41
CXOM31 J004226.1+412551	00 42 26.11	+41 25 51.0	2.6 ± 0.06	2.1 ± 0.06	Bo7	31.79	0.001	…	0.47
CXOM31 J004255.3+412558	00 42 55.31	+41 25 58.0	…	…	…	…	…	…	3.79
CXOM31 J004353.6+411654	00 43 53.62	+41 16 54.0	4.5 ± 0.10	2.2 ± 0.10	Bo7	10.83	0.543	GC	4.08
CXOM31 J004303.1+411015	00 43 03.08	+41 10 16.1	2.4 ± 0.08	2.3 ± 0.08	Bo138	4.84	0.963	GC	2.84

NOTE.—Units of right ascension are hours, minutes, and seconds, and units of declination are degrees, arcminutes, and arcseconds.

as a single Gaussian. Here we use a homoscedastic test; i.e., the two Gaussians are assumed to have the same dispersion. The m_v of the two peaks are 15.65 and 17.89, the P-value is 0.094, and the number of GC X-ray sources assigned to each peak by the KMM test are 44 and 14, respectively. The P-value is in fact the probability that the data are drawn from a single-Gaussian distribution. The KMM test suggests that we can consider the distribution to be bimodal at the 90.6% confidence level. At the same time, we use a Kolmogorov-Smirnov (KS) test to demonstrate whether the two distributions in Figure 5 are the same. We determined a value of $D_{max} = 0.354$ for these two samples, which have 58 and 333 points, respectively. The probability of obtaining a value of $D_{max} = 0.354$ for 58 and 333 points is less than 10^{-5}. We can reject the hypothesis that the two distributions are the same at the 100% confidence level. In addition, the KS test determined a value of $D_{max} = 0.566$ for the distribution of GC X-ray sources between those listed in Trudolyubov & Priedhorsky (2004) and those given here. The probability of obtaining a value of $D_{max} = 0.566$ for 6 and 15 points is 7.89%. We can reject the hypothesis that the two distributions are the same at the 90% confidence level. In the latter KS test, we used the numbers from X-ray GCs in various bins, since Trudolyubov & Priedhorsky (2004) did not list the values of V magnitude provided in Table 3, so the numbers are normalized; i.e., in each bin the number of objects is divided by the number of all the objects.

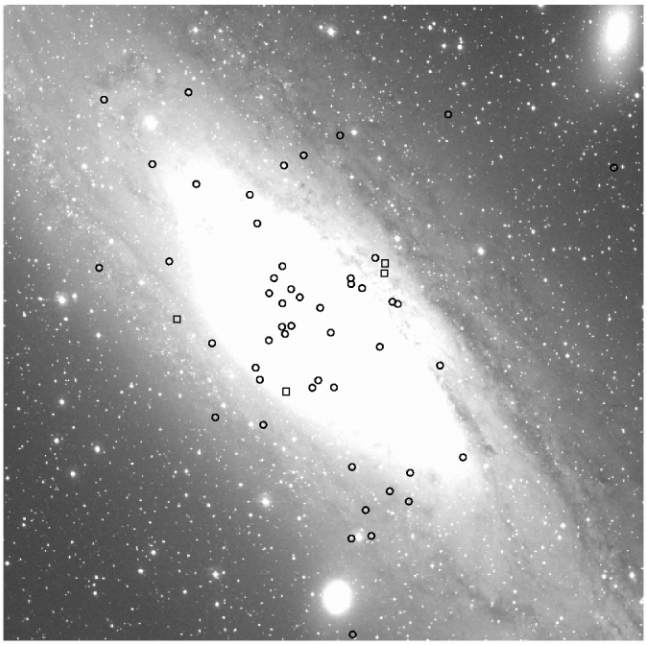

FIG. 4.—Position distributions of the GC X-ray sources in the BATC M31 field. The circles represent the known GC X-ray sources, while the squares represent the newly identified GC X-ray candidates

In Figure 6, we plot the $B - V$ color and V magnitude for the GC candidates of X-ray sources. We do not see any evident difference with the data in Figure 5 of Battistini et al. (1987).

Using a sample of four early-type galaxies with X-ray sources, Sarazin et al. (2003) found a tendency for X-ray sources to occur preferentially in redder GCs, which seems to indicate that the evolution of X-ray binaries in GCs is affected by either the metallicity or the age of the GC (Sarazin et al. 2003). Figure 7 plots the distribution of $B - V$ color for the GC candidates of X-ray sources, and also the A and B class GC candidates from Battistini et al. (1987). For clarity, we also use the normalized number used in Figure 5. This shows that the GC X-ray sources seem to be associated preferentially with the redder GCs, in agreement with the results of Sarazin et al. (2003). In order to determine whether GC X-ray sources and GCs are drawn from the same distribution, we also provide the KS test. We determined a value of $D_{max} = 0.181$ for these two samples, with 58 and 328 points, respectively. The probability of obtaining a value of $D_{max} = 0.181$ for 58 and 328 points is 6.8%, which means we can reject the hypothesis that the two distributions are the same at the 90% confidence level.

5.3. Correlation between X-Ray and Optical Luminosity for the GC Candidates of X-Ray Sources in M31

Since the clusters of galaxies show a close correlation between total optical luminosity and X-ray luminosity, $L_{opt} \propto$

TABLE 6
THE PARAMETERS OF 62 X-RAY GC CANDIDATES

Source ID (1)	Optical ID[a] (2)	X-ray ID[b] (3)	L_X[c] (10^{35} ergs s^{-1}) (4)	V[d] (5)	$B-V$[d] (6)
1[f]	G1		6	…	…
2[f]	Bo293	RX J0036.3+4053	5.1	16.39	0.45
3[f]	Bo5	SHP73	1990	15.67	1.02
4[f]	MA94a(16)	RX J0040.5+4033	9.0	…	…
5	Bo7	RX J0040.4+4129	71.5	14.25 ± 0.003	0.50 ± 0.006
6	MIT87	D27	3	18.99 ± 0.129	1.02 ± 0.220
7	Bo45	RX J0041.7+4134	450	15.74 ± 0.008	0.90 ± 0.022
8[f]	Bo58/MIT106	D22	1–24	15.06	0.80
9	Bo55		2.4–2.9	16.67 ± 0.031	1.55 ± 0.117
10	Bo D42/MIT130	SHP138, D13	31–73	18.62 ± 0.092	0.94 ± 0.120
11	Bo D44	D15	40–100	18.45 ± 0.085	1.24 ± 0.211
12	MIT140	D10	40–114	16.78 ± 0.064	1.64 ± 0.158
13	Bo78/MIT153	D20	24–300	17.65 ± 0.199	1.71 ± 0.378
14	Bo82/MIT159	SHP150, D2	1735–2330	15.48 ± 0.009	1.71 ± 0.040
15[e]		CXOM31 J004215.0+412122	3	18.31 ± 0.085	0.74 ± 0.105
16[e]		CXOM31 J004215.5+412031	26	18.64 ± 0.219	0.57 ± 0.268
17	Bo86/MIT164	SHP158, D4	498–763	14.97 ± 0.043	0.72 ± 0.058
18	MIT165/MIT166	D24	5	18.23 ± 0.133	1.66 ± 0.440
19	Bo94/MIT173	SHP168, D21	19	15.52 ± 0.010	0.83 ± 0.020
20	Bo98	D25	1–12	16.19 ± 0.008	0.84 ± 0.011
21	Bo96/MIT174	D14	28–174	16.11 ± 0.109	1.20 ± 0.166
22	Bo D63	[WGK2004]s1-83	154	18.52 ± 0.104	0.54 ± 0.182
23	Bo110	SHP178	41–52	15.13 ± 0.008	0.81 ± 0.015
24	Bo117		14	16.22 ± 0.032	0.70 ± 0.046
25	Bo107/MIT192	SHP175, D16	56–290	15.83 ± 0.081	0.93 ± 0.114
26	NBol 63	CXOM31 J004231.2+412008	5	16.73 ± 0.170	0.74 ± 0.209
27	Bo116	RX J0042.5+4132	234	16.79 ± 0.023	1.37 ± 0.091
28	Bo123/MIT212	D18	16–27	17.28 ± 0.199	0.98 ± 0.279
29	MIT213	D23	34–137	13.25 ± 0.164	1.06 ± 0.225
30	PB-in7	CXOM31 J004246.0+411736	9	14.66 ± 0.273	1.00 ± 0.359
31	Bo128	[PFJ93]51	237	16.84 ± 0.107	0.85 ± 0.142
32[g]	MIT222	D28	3	…	…
33	Bo135	SHP205	3093–4009	15.89 ± 0.012	0.92 ± 0.027
34	Bo138		8–84	15.84 ± 0.206	0.97 ± 0.282
35	Bo144	D6	216–512	15.98 ± 0.251	1.00 ± 0.329
36	Bo143	SHP217, D5	152–555	15.89 ± 0.099	0.85 ± 0.128
37[e]		CXOM31 J004303.1+411015	62	15.29 ± 0.008	1.05 ± 0.011
38	Bo146	SHP220, D7	74–414	16.81 ± 0.331	0.81 ± 0.426
39	Bo D91/MIT236	SHP218	553–692	14.26 ± 0.005	1.44 ± 0.012
40	Bo147/MIT240	SHP222, D11	52–194	15.52 ± 0.057	0.90 ± 0.082
41	Bo148	SHP223, D8	105–418	15.77 ± 0.097	0.78 ± 0.123
42	[WSB85] S3 14	CXOM31 J004304.2+411601	43	16.61 ± 0.180	0.86 ± 0.240
43	Bo150/MIT246	D19	16–72	16.24 ± 0.097	1.08 ± 0.158
44	[WSB85] S1 4	CXOM31 J004309.7+411901	212	17.86 ± 0.283	1.55 ± 0.530
45	Bo153/MIT251	SHP228, D3	373–1248	16.09 ± 0.084	1.02 ± 0.120
46	Bo158	SHP229, D12	600–1880	14.60 ± 0.004	0.88 ± 0.009
47	Bo161/MIT260	D26	16–22	16.23 ± 0.035	0.86 ± 0.056
48	Bo159		2	16.96 ± 0.063	1.20 ± 0.128
49	Bo164/MA94a (269)	RX J0043.2+4112	13	17.68 ± 0.115	0.95 ± 0.186
50	Bo163	RX J0043.2+4127	1–1010	15.00 ± 0.008	0.98 ± 0.016
51	Bo182		46	15.35 ± 0.007	0.96 ± 0.017
52	Bo185/MIT299	SHP247, D9	454–1981	15.49 ± 0.011	0.91 ± 0.021
53	MIT311	SHP250	52	18.34 ± 0.121	1.14 ± 0.350
54	Bo193	SHP253	44	15.33 ± 0.008	0.95 ± 0.017
55[e]		CXOM31 J004353.6+411654	305	18.22 ± 0.112	0.40 ± 0.145
56	Bo204	SHP261	37	15.66 ± 0.010	0.86 ± 0.022
57	Bo213	2E 0041.3+4114	201	16.98 ± 0.024	0.74 ± 0.034
58	MA94a (380)	RX J0044.4+4136	27	14.72 ± 0.005	0.87 ± 0.011
59	Bo225	SHP282	1130	14.13 ± 0.003	0.87 ± 0.007

TABLE 6 (*Continued*)

Source ID (1)	Optical ID[a] (2)	X-ray ID[b] (3)	L_X[c] (10^{35} ergs s^{-1}) (4)	V[d] (5)	$B-V$[d] (6)
60[f]	MA94a (447)	RX J0045.4+4132	15	...	...
61[f]	Bo375	SHP318, D1	5148–10372	17.54	1.47
62[f]	Bo386	SHP349	1496	15.59	0.76

[a] Source identifications beginning with Bo refer to the GC candidates listed in Battistini et al. (1987); Bo D to the GC candidates listed in Battistini et al. (1980); MIT in Magnier (1993); MA94a in Magnier et al. (1994); NBol in Battistini et al. (1993); and PB in Barmby (2001).

[b] Source identifications beginning with SHP refer to M31 *ROSAT*/PSPC X-ray source catalog entries in Supper et al. (1997, 2001); D refers to Di Stefano et al. (2002b); 2E to Barmby et al. (2000); [PFJ93] to Primini et al. (1993); [WGK2004] to Williams et al. (2004); and [WSB85] to Wirth et al. (1985).

[c] Numbers 2, 4, 5, 7, 49, 58, and 60 are in the 0.1–2 keV range, numbers 15, 26, and 30 are 0.3–7 keV, numbers 16, 22, 27, 37, 42, 44, and 55 are 0.1–10 keV, and numbers 31 and 57 are 0.2–4.0 keV. The others are 0.3–10.0 keV.

[d] V magnitudes and $B-V$ colors with error bars are from the BATC; those without error bars are from Battistini et al. (1987).

[e] The new X-ray GC candidates identified in this paper.

[f] The sources are outside of the BATC M31 field.

[g] The sources are in the BATC M31 field but cannot be detected because of low S/N.

$L_X^{0.45\pm0.03}$ (Popesso et al. 2004), we wonder whether a similar correlation exits between optical luminosity and X-ray luminosity for GC X-ray sources. The X-ray luminosities of 62 sources are taken from several different observations in different energy bands. Thus, we have to use the 43 X-ray GC candidates from Trudolyubov & Priedhorsky (2004) that were observed in the 0.3–10 keV energy band. A large number of X-ray GC sources have wide-ranging X-ray luminosities, so we use error bars in Figure 8 to show the X-ray luminosity range used by Trudolyubov & Priedhorsky (2004). Furthermore, in Figure 8 a 10% uncertainty in X-ray luminosity for some sources is accepted, which is translated directly from the uncertainty ($\pm10\%$) in flux reported by Trudolyubov & Priedhorsky (2004). There are only two candidates for which the V magnitudes cannot be obtained (see § 5.2 for details). Figure 8 therefore shows the correlation between X-ray luminosity and V magnitude for 41 GC X-ray sources. In order to present a quantitative analysis, we do an ordinary least-

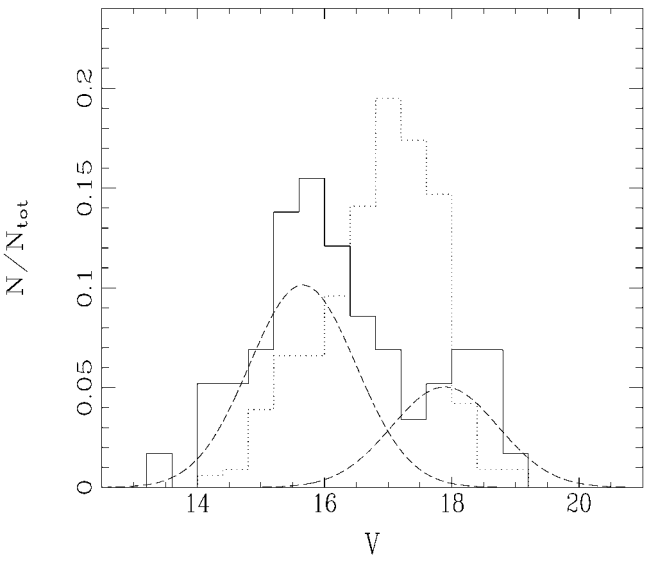

FIG. 5.—V magnitude distributions of GC X-ray sources and all the GC candidates in M31. The results for the GC X-ray sources are shown by a solid histogram. The distribution for the GC candidates from Battistini et al. (1987) is shown with a dotted histogram. The dashed lines show the bimodal fitting of V magnitude distribution of GC X-ray sources, according to the KMM test.

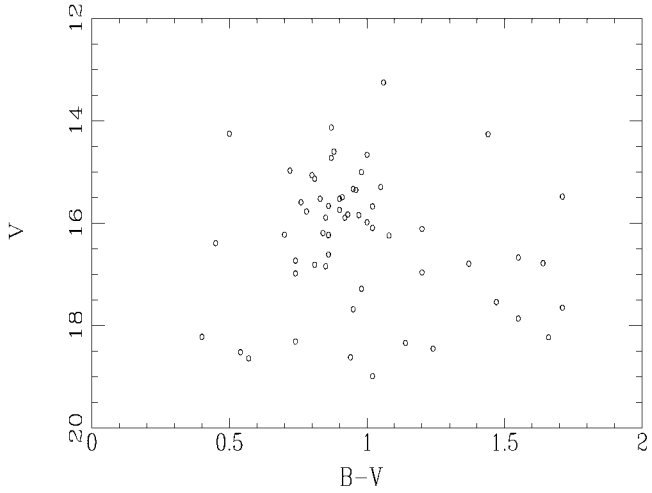

FIG. 6.—$B-V$ color and V magnitude diagram for the GC X-ray sources in M31.

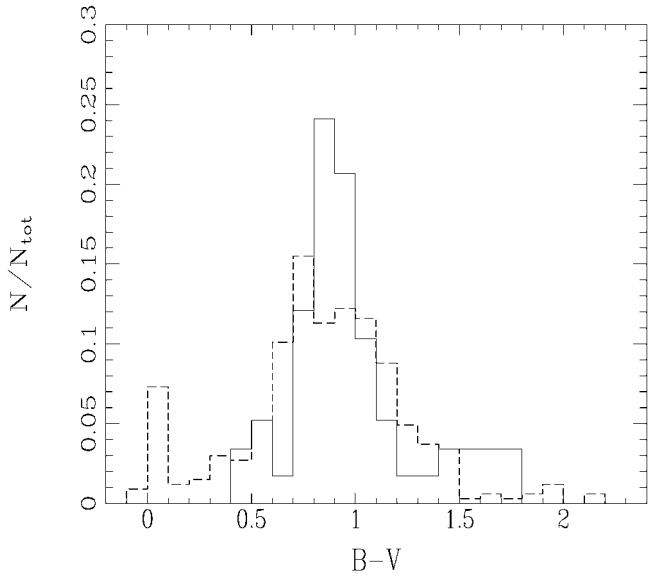

FIG. 7.—The $B - V$ color distributions of the GC X-ray sources and the GC candidates in M31. The results for the GC X-ray sources are shown with a solid line histogram. The distribution for the GC candidates from Battistini et al. (1987) is shown with a dashed histogram.

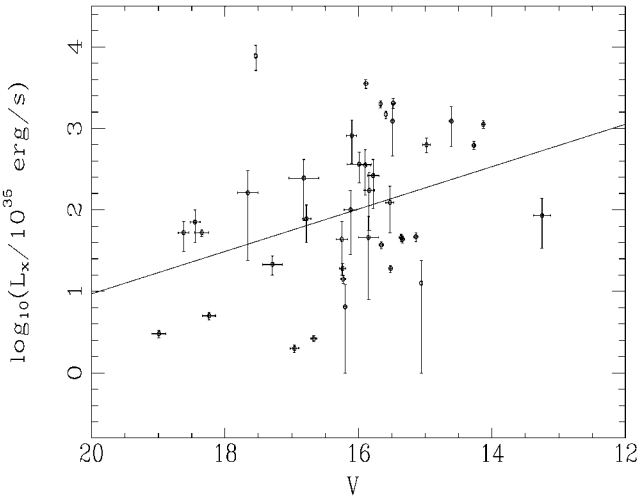

FIG. 8.—Correlation between X-ray luminosities and V magnitudes for the GC X-ray sources in M31.

squares fit. The fitting formula is

$$\log (L_{\rm X}/10^{35}) = a\, m_v + b, \qquad (7)$$

and the fitting results are $a = -0.26 \pm 0.11$, $b = 6.17 \pm 1.76$, and a linear correlation coefficient $r = 0.36$ at a confidence level of 98.0%. If our sample were to exclude source number 61 in Table 6, the fitting results would be much better: $a = -0.31 \pm 0.10$, $b = 6.96 \pm 1.64$, and a linear correlation coefficient of $r = 0.45$ at a 99.5% confidence level.

6. SUMMARY

In this paper, we study the properties of GC X-ray sources. First, we identify the optical counterparts of the X-ray point sources in M31, using the results of the *Chandra* ACIS-I and HRC observations from 1999 to 2001, *Einstein* observations from 1979 to 1980, and *ROSAT* HRI observations in 1990, in addition to data from the BATC optical survey from 1995 to 1999. We identify eight new optical counterparts of X-ray point sources, and by analyzing both the SEDs and FWHMs, find that four of them are probably GC candidates. Second, we collect 62 GC X-ray sources, 53 of which have SEDs that are from 4000 to 10000 Å. The V magnitudes and $B - V$ colors are obtained using the BATC optical survey from 1995 to 1999. We then determine some statistical relationships between the GC X-ray sources. The results show that the distribution of V magnitude in the GC X-ray sources and GC candidates are different. The majority of GC X-ray sources are brighter than 17 mag, which is the peak of the distribution of the GC candidates. At the same time, the V distribution of the GC X-ray sources in M31 is bimodal, with peaks at $m_v = 15.65$ and 17.89. The distribution of $B - V$ color of GC X-ray sources and GC candidates from Battistini et al. (1987) show that the GC X-ray sources seem to be associated preferentially with the redder GCs, in agreement with previous results, and a KS test shows that the maximum value of the absolute difference of these two distributions is $D_{\rm max} = 0.181$, with $P = 0.068$. Finally, we study the correlation between X-ray luminosity (0.3–10 keV) and optical luminosity (V magnitude) and find that there exists a weak relationship, with a linear correlation coefficient $r = 0.36$ at a confidence level of 98.0%.

We would like to thank the anonymous referee for his/her insightful comments and suggestions, which greatly improved this paper. This work has been supported by the Chinese National Key Basic Research Science Foundation (NKBRSF TG199075402) and by the Chinese National Natural Science Foundation, number 10473012.

REFERENCES

Ashman, K. A., Bird, C. M., & Zepf, S. E. 1994, AJ, 108, 2348
Barmby, P. 2001, Ph.D. thesis, Harvard Univ.
Barmby, P., Huchra, J., Brodie, J., Forbes, D., Schroder, L., & Grillmair, C. 2000, AJ, 119, 727
Battistini, P., Bònoli, F., Braccesi, A., Federici, L., Fusi Pecci, F., Marano, B., & Börngen, F. 1987, A&AS, 67, 447
Battistini, P., Bònoli, F., Braccesi, A., Fusi Pecci, F., Malagnini, M. L., & Marano, B. 1980, A&AS, 42, 357
Battistini, P. L., et al. 1993, A&AS, 272, 77
Bellazzini, M., Pasquali, A., Federici, L., Ferraro, F. R., & Fusi Pecci, F. 1995, ApJ, 439, 687
Berkhuijsen, E. M., Humphreys, R. M., Ghigo, F. D., & Zumach, W. 1988, A&AS, 76, 65
Clark, G. W. 1975, ApJ, 199, L143
Collura, A., Reale, F., & Peres, G. 1990, ApJ, 356, 119
Di Stefano, R., Greiner, J., Murray, S., & Garcia, M. 2002a, ApJ, 570, 618
Di Stefano, R., Kong, A. K. H., Garcia, M. R., Barmby, P., Greiner, J., Murray, S. S., & Primini, F. A. 2002b, ApJ, 570, 618
Di Stefano, R., Kong, A. K. H., VanDalfsen, M. L., Harris, W. E., Murray, S. S., & Delain, K. M. 2003, ApJ, 599, 1067
Fabian, A. C., Pringle, J. E., & Rees, M. J. 1975, MNRAS, 172, 15
Fan, X., et al. 1996, AJ, 112, 628
Ford, H. C., & Jacoby, G. H. 1978, ApJS, 38, 351
Fukugita, M., et al. 1996, AJ, 111, 1748
Galadí-Enríquez, D., Trullols, E., & Jordi, C. 2000, A&AS, 146, 169
Galleti, S., et al. 2004, A&A, 416, 917
Hertz, P., & Grindlay, J. E. 1983, ApJ, 275, 105
Kaaret, P. 2002, ApJ, 578, 114
Kong, A. K. H., et al. 2002, ApJ, 577, 738
Lampton, M., Margon, B., & Bowyer, S. 1976, ApJ, 208, 177
Landolt, A. U. 1983, AJ, 88, 439
———. 1992, AJ, 104, 340
Liu, Q. Z., van Paradijis, J., & van den Heuvel, E. P. J. 2001, A&A, 368, 1021
Macri, L. M. 2001, ApJ, 549, 721
Magnier, E. 1993, Ph.D. thesis, Mass. Inst. Tech.
Magnier, E. A., et al. 1994, A&AS, submitted
Murray, S. S., et al. 1997, Proc. SPIE, 3114, 11
Oke, J. B., & Gunn, J. E. 1983, ApJ, 266, 713
Osborne, J. P., et al. 2001, A&A, 378, 800
Popesso, P., et al. 2004, A&A, 423, 449
Primini, F. A., Forman, W., & Jones, C. 1993, ApJ, 410, 615
Sarazin, C. L., Kundu, A. I., Irwin, J. A., Sivakoff, G. R., Blanton, E. L., & Randall, S. W. 2003, ApJ, 595, 743
Sidoli, L., Parmar, A. N., Oosterbroek, T., Stella, L., Verbunt, F., Masetti, N., & Dal Fiume, D. 2001, A&A, 368, 451
Stanek, K. Z., & Garnavich, P. M. 1998, ApJS, 503, 131
Stetson, P. B. 1987, PASP, 99, 191
Supper, R., Hasinger, G., Lewin, W. H. G., Magnier, E. A., van Paradijs, J., Pietsch, W., Read, A. M., & Trümper, J. 2001, A&A, 373, 63
Supper, R., Hasinger, G., Pietsch, W., Trümper, J., Jain, A., Magnier, E. A., Lewin, W. H. G., & van Paradijs, J. 1997, A&A, 317, 328
Trinchieri, G., & Fabbiano, G. 1991, ApJ, 382, 82
Trinchieri, G., et al. 1999, A&A, 348, 43
Trudolyubov, S., & Priedhorsky, W. 2004, ApJ, 616, 821
van Speybroeck, L., Epstein, A., Forman, W., Giacconi, R., Jones, C., Liller, W., & Smarr, L. 1979, ApJ, 234, L45
Verbunt, F., Bunk, W., Hasinger, G., & Johnston, H. 1995, A&A, 300, 732
Williams, B. F., et al. 2004, ApJ, 609, 735
Wirth, A., Smarr, L. L., & Bruno, T. L. 1985, ApJ, 290, 140
Wu, H., et al., 2002, AJ, 123, 1364
Yan, H. J., et al. 2000, PASP, 112, 691
Zheng, Z. Y., et al. 1999, AJ, 117, 2757
Zhou, X., Jiang, Z. J., Xue, S. J., Wu, H., Ma, J., & Chen, J. S. 2001, Chinese J. Astron. Astrophys., 1, 372
Zhou, X., et. al. 2003, A&A, 397, 361
———. 2004, AJ, 127, 3642